Article

Thermogravimetric Kinetic Analysis of Non-Recyclable Waste CO₂ Gasification with Catalysts Using Coats–Redfern Method

Ahmad Mohamed S. H. Al-Moftah [1,2,*]📀, **Richard Marsh** [1] **and Julian Steer** [1]📀

1   Cardiff School of Engineering, Cardiff University, Queen's Buildings, The Parade, Cardiff CF24 3AA, UK; marshr@cardiff.ac.uk (R.M.); steerj1@cardiff.ac.uk (J.S.)
2   Qatar National Research Fund, Qatar Foundation, Doha P.O. Box 5825, Qatar
*   Correspondence: al-moftaha@cardiff.ac.uk

Abstract: In the present study, the effect of dolomite and olivine as catalysts on the carbon dioxide (CO₂) gasification of a candidate renewable solid recovered fuel, known as Subcoal™ was determined. Thermogravimetric analysis (TGA) was used to produce the TGA curves and derivative thermogravimetry (DTG) for the gasification reaction at different loadings of the catalyst (5, 10, 15 wt.%). The XRD results showed that the crystallinity proportion in Subcoal™ powder and ash was 42% and 38%, respectively. The Arrhenius constants of the gasification reaction were estimated using the model-fitting Coats–Redfern (CR) method. The results showed that the mass loss reaction time and thermal degradation decreased with the increase in catalyst content. The degradation reaction for complete conversion mainly consists of three sequences: dehydration, devolatilisation, and char/ash formation. The complete amount of thermal degradation of the Subcoal™ sample obtained with dolomite was lower than with olivine. In terms of kinetic analysis, 19 mechanism models of heterogeneous solid-state reaction were compared by the CR method to identify the most applicable model to the case in consideration. Among all models, G14 provided excellent linearity for dolomite and G15 for olivine at 15 wt.% of catalyst. Both catalysts reduced the activation energy (E_a) as the concentration increased. However, dolomite displayed higher CO₂ gasification efficiency of catalysis and reduction in E_a. At 15 wt.% loading, the E_a was 41.1 and 77.5 kJ/mol for dolomite and olivine, respectively. Calcination of the mineral catalyst is substantial in improving the activity through enlarging the active surface area and number of pores. In light of the study findings, dolomite is a suitable mineral catalyst for the industrial-scale of non-recyclable waste such as Subcoal™ gasification.

Keywords: non-recyclable waste; Subcoal™; non-isothermal; olivine; dolomite; TGA; CO₂ gasification; Qatar national vision 2030

1. Introduction

Climate change and global warming from the emission of greenhouse gases (GHG) are currently defined as major threats to humanity. A series of international measures and actions have been taken to mitigate the GHG effect. Recently, in Glasgow, the 26th UN Climate Change Conference of the Parties (COP26) was conducted. The participants emphasised the commitment to deep GHG emissions cuts and support the 1.5 °C global warming limit goal [1]. One of the most effective ways to cut emissions is using the thermal conversion of sustainable biomass into energy, where this biomass is assumed to utilise renewable carbon within its lifecycle.

Municipal solid waste (MSW) is one of the most inexpensive and available alternative fuels. The landfilling of non-recycled MSW in some countries such as Qatar is a challenging disposal method due to the lack of land and emissions from landfills [2]. Alternatively to landfill, the non-recycled MSW in Qatar can potentially be gasified to produce valuable synthesis gas (syngas) consisting of CO, CO₂, CH₄, and H₂ [3].

The study herein was driven by the Qatar National Vision 2030 for better MSW management. Adopting biomass gasification in Qatar will minimise the air pollutants emitted from the combustion of fossil fuels and landfills. Currently, the Domestic Solid Waste Management Centre (DSWMC) in Doha generates 30 MW of electricity from MSW as a part of the Waste-to-Energy (WtE) program [4].

Subcoal™ is a promising fossil fuel substitute consisting of a non-recyclable mixture of plastics and paper waste and is produced by the N + P Group [5]. It comes with unique properties such as high energy content, low sulphur content, and good hydrophobicity. Due to these properties, this material has been used as a solid fuel in different industries such as steel and cement production. The kinetics of Subcoal™ gasification have received limited attention in the reported literature [6]. It can be prepared from the MSW in Qatar as a feedstock for a gasification plant.

Biomass fluidised bed gasification takes place widely over bed materials, which are a mixture of sand and catalyst particles. However, the production of tar during gasification may lead to serious problems in the system such as condensation and clogging, therefore, a tar removal method is usually required [7]. In the case of municipal solid waste, the amount of material involved is likely to be very large, so the reactor residence time and length scales are the major design criteria of technical interest [2]. Therefore, a catalyst is necessary to enhance the reaction for the production of syngas. Another role of the catalyst is the cracking of tar including thermal and hydrocracking [5]. The hydrocarbons are adsorbed in their dissociative form after hydrogen is removed catalytically [6].

Synthetic and natural catalysts have been used in biomass gasification. Natural mineral catalysts are found in the Earth's crust such as dolomite and olivine [8–10]. They are commonly used because they are abundantly available and are inexpensive compared to refined and precious metals [8]. The formation of dolomite in the Khor Al-Adaid sabkha in Qatar has been reported in the work of DiLoreto et al. [11].

Olivine is a rock-forming mineral that is naturally available with a general chemical formula of magnesium iron silicate $(Mg_x, Fe1-x)_2 SiO_4$. The catalytic activity of olivine for tar reduction can be related to iron oxide (Fe_2O_3), magnesite (MgO), and nickel (Ni) portions. Iron is effective when it is found on the surface of the catalyst. Oxidation and/or calcination of olivine helps to transfer iron to the surface. Olivine is mainly deactivated by the formation of coke, which covers the active sites and reduces the surface area of a catalyst [12]. The catalytic influence of olivine on biomass gasification has been examined in several studies [13–16].

Dolomite is a widespread inexpensive mineral that forms in rocks over a significant underground area. It is a common tar conversion catalyst that is composed of calcium magnesium carbonate $CaMg(CO_3)_2$ [17,18]. The composition of dolomite may vary depending on the geographical location [19], however, the major compounds found in dolomite are calcium oxide (CaO), magnesium oxide (MgO), and CO_2 [20]. Dolomite may also contain traces of silica (SiO_2), aluminium oxide (Al_2O_3), and Fe_2O_3 [21].

This paper aimed to investigate the effects of dolomite and olivine concentrations on the Subcoal™ CO_2 gasification using TGA. The XRD data of Subcoal™ fuel and ash will be provided as part of the catalytic effect investigation. The thermal behaviour and kinetic parameters in the presence of the catalyst will be examined using the Coats–Redfern (CR) method. In addition, this study is regarded as foundational knowledge for future Subcoal™ gasification with catalyst research. However, this paper aimed to investigate the effects of mineral-based catalysts, namely, dolomite and olivine on the Subcoal™ CO_2 gasification using TGA. Subcoal™ as a fuel is a novel and new material type that is segregated from municipal solid waste (MSW), which can be used effectively in gasification technology to generate power in countries suffering from MSW landfilling and fossil fuel emissions such as in Qatar. In our previous studies, we presented the behaviour and kinetics of uncatalysed Subcoal™ gasification using a model free method. Some mineral catalysts such as dolomite and olivine are abundant in the Middle East region. It would be useful to achieve an understanding of the catalysis performance of these minerals in the gasification

process. The influence of inexpensive mineral catalysts on the gasification of Subcoal has received insufficient or no attention. This is the first study that also included reaction kinetics investigations, which contribute to the better design of a Subcoal™ gasifier in the presence of CO_2 and a mineral catalyst. CO_2 as a gasifying agent offers unique features over air or steam to ensure better gasification performance and as a way of CO_2 utilisation. Finally, the present study is regarded as foundational knowledge for future Subcoal™ gasification with catalyst research.

2. Methodology

2.1. Materials

Pulverised Subcoal™ pellets are a commercially available waste-derived material made of non-recyclable paper and plastic waste [22]. A sample of this material was provided by N + P Group B.V in the Netherlands. To study the effect of catalyst loadings on Subcoal™ by TGA, pulverised Subcoal™ pellets were milled to less than 3 mm using a knife mill grinding machine (Fritish GmbH, Idar-Obersten, Germany). This milled product is known as a pulverised alternative fuel (PAF). The mineral content in the Subcoal™ ash (as received) was determined using X-ray fluorescence (XRF), as shown in Table 1. The minerals and elements in ash may potentially provide catalytic effects on the gasification reaction [23].

Table 1. XRF analysis of the major minerals in Subcoal™ ash.

Elements	Al_2O_3	CaO	Fe_2O_3	K_2O	SiO_2
wt.%	18.3	38	2.7	0.1	22.7

The XRD analysis of Subcoal™ powder <3 mm and ash were carried using X-ray diffraction (Diffraktometer D5000, Siemens, Munich, Germany) with a 2θ range of 20° to 90° to identify the crystallinity and composition. The sample was mounted on the diffractometer sample holder in a flat layout. A typical sample holder is a 2 mm thick plate with a 20 mm square hole in the centre. The proportion of the crystalline components in the fuel (crystallinity) was determined according to standard test method ASTM D5758 and results evaluated using the following formula [24]:

$$\text{Crystallinity \%} = \frac{A_c}{A_c + A_a} \times 100 \qquad (1)$$

where A_c is the area under the peaks representing the total crystalline region, and A_a is the area under the peaks representing the total amorphous region [24]. In addition, the sample was placed onto the holder in the machine sample stage and compressed using a glass slide to obtain a flat and even surface. The holder was transferred into the XRD goniometer and the door was closed. The chiller unit and XRD unit were then switched on, respectively. The default power was set at 200 W (20 mA and 10 kV), which was increased to 1400 W (35 mA and 40 kV). The shutter door was kept open to allow X-rays to reach the sample. Then, the scanned data were inserted in the computer-based software (Panalytical X'Pert HighScore Plus) that organises the scanning process. Finally, the scan program was sent to the XRD machine and the scan commenced. The results were transferred to OriginPro® software and the crystallinity of the sample was calculated.

The XRD analysis of the Subcoal™ powder produced a large peak of amorphous compounds at 2θ of 23° composed of barium (Ba), calcium (Ca), and silica (Si), as shown in Figure 1. The first amorphous peak compounds consisted mainly of Ba, Ca, and Si. The next peak confirmed a crystalline compound at 27° with an intensity of 161 a.u. while the second amorphous peak appeared at 30°. Previous research in this area, specifically in relation to the analysis of polymers with XRD, by Marsh [25] found that amorphous peaks were dominant, as shown by their defined peaks. However, the amount of crystalline matters in plastic and paper waste exceeded the randomly distributed amorphous ones.
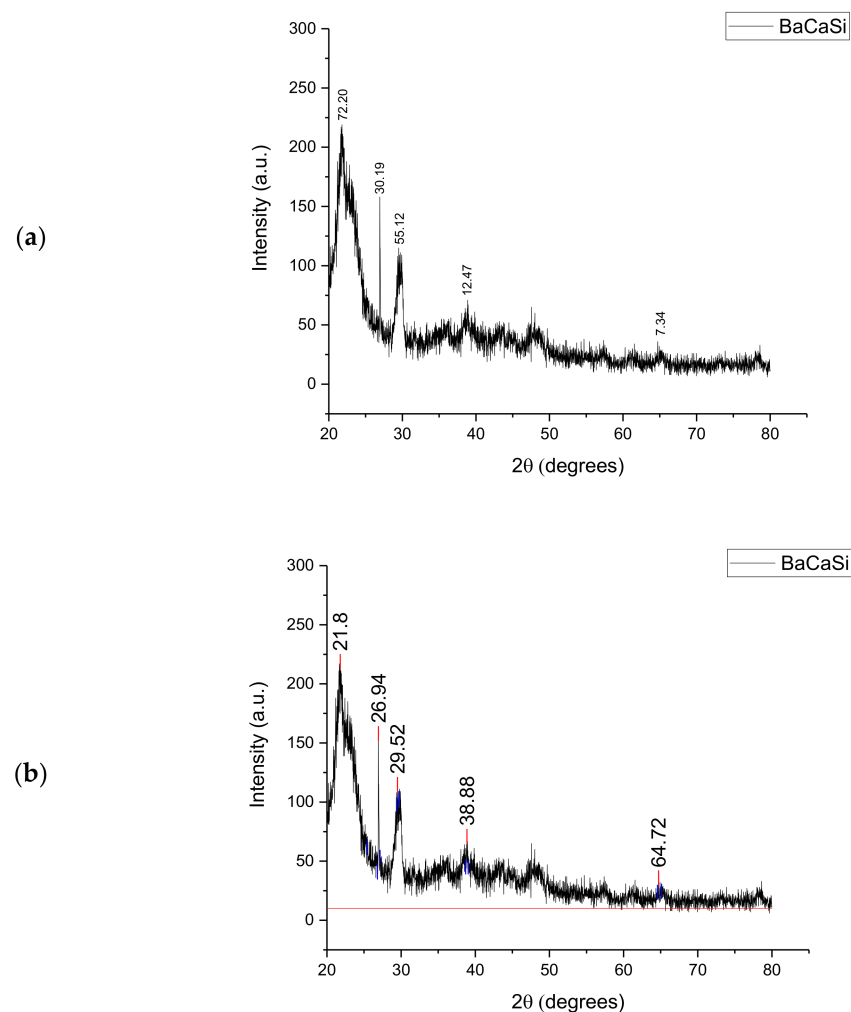
Figure 1. XRD analysis of the Subcoal™ powder: (**a**) peak height, and (**b**) peak area. The red line has been added to calculate the area under the curve.

Small crystalline peaks appeared at 2θ of 40° and 65° with the intensity of 75.5 and 26.5 au., respectively, which consisted of trace elements. It was found that the crystallinity proportion in Subcoal™ powder based on the total area of all peaks was 42%. XRD is also a substantial tool for the semi-quantitative evaluation of crystalline phases and mineral components in ash [26]. The content of amorphous materials in the biomass sample or ash determines the decomposition temperature. The higher the glass (amorphous) content, the lower the gasification temperature [27]. The non-crystallinity is attributed to the presence of amorphous aluminosilicate [28].

Figure 2 shows the XRD analysis of Subcoal™ ash in terms of peak height (a) and area (b) that was used to identify the crystallinity of the sample. The area of a peak is calculated by multiplying the FWHM (full width at half maximum) times the height. The area under the peak provides information on the percentage of crystallinity. The height of the main peaks indicates the intensity of each polymorphic phase. The largest crystalline peak of calcium chloride (CaCl) was obtained at 38.5° with an intensity of 245 au. Semi-crystalline peaks were also detected between 30° and 35°. The remaining signals included small crystalline peaks and experimental noise. The crystallinity percentage in ash based on the total area of all peaks was found to be 37.67%. In comparison with the Subcoal™ sample, the reduction in the crystallinity can be attributed to the decomposition of crystalline cellulose fibres [29]. The crystalline minerals and metal oxides in the ash may behave as a catalyst of thermal decomposition reactions [30].
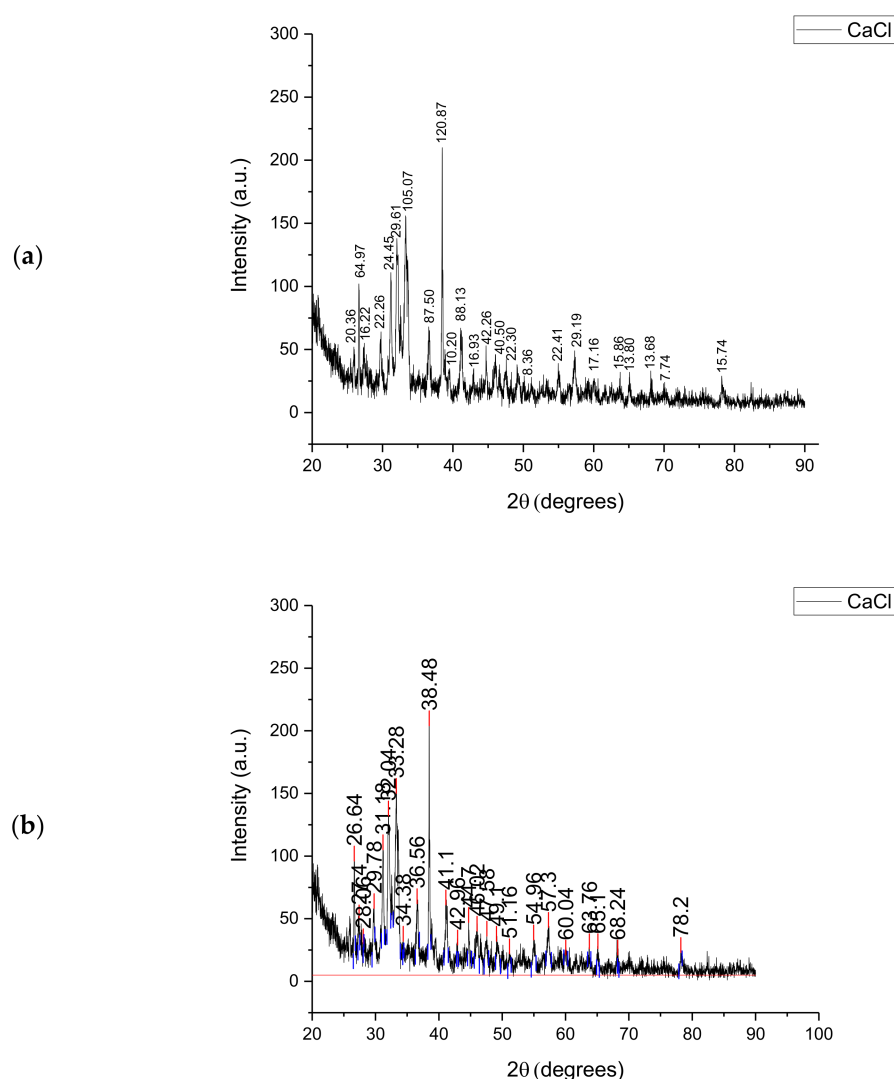
Figure 2. XRD analysis of the Subcoal™ ash: (**a**) peak height, and (**b**) peak area. The red line has been added to calculate the area under the curve.

Dolomite and olivine were supplied by the Tarmac Company (Solihull, UK) from Port Talbot in the form of powder with a particle size of <1 mm. Catalyst particle size was reduced and sieved to 106–212 μm according to BS 1377-9:1990 using a ring mill machine (Labtech Essa 100100, Australia). The chemical composition of olivine and dolomite is listed in Table 2 as supplied by the manufacturer. As can be seen, the dispersion of the active species (CaO and MgO) on the dolomite and olivine particles were around 48.72% and 49.26%, respectively.

2.2. Experimental Procedure

The experiments of CO_2 gasification of Subcoal™ were carried out at Cardiff University using TGA (Mettler Toledo AG TGA/SDTA 851e, USA). CO_2 converts char (carbon) to CO according to the slightly endothermic Boudouard reaction, which is favourable at high temperature [31]. However, using air as a gasifying agent leads to syngas dilution with nitrogen, which reduces the heating value of the fuel gas. In contrast to steam, CO_2 requires no heat for water evaporation [32]. The gasification study in TGA provides data on the thermal decomposability of Subcoal™ in relatively less expensive and complex experiments. Under non-isothermal conditions, TGA and DTG analysis were conducted for a temperature range of 25 to 900 °C following the BS EN ISO 11358:1997 standard. A constant heating rate of 20 °C/min was adopted to test the influence of different catalyst

loadings (0%, 5%, 10%, and 15% on a weight basis). However, low loadings of the catalyst (e.g., 1 wt.%) were considered in this study due to insignificant changes in the gasification performance that is due to poor mixing with Subcoal and the gasification agent. A 10 ± 5 mg of a Subcoal™ PAF sample was placed into a cylindrical alumina crucible. The crucible and sample were loaded onto the TGA carousel using tweezers. CO_2 was used as a gasifying agent with a flow rate of 100 mL/min [26]. The weight loss was recorded against the time and temperature to produce TGA and DTG curves. Once the experiment was completed, the temperature, time, and mass change data were exported to a spreadsheet.

Table 2. Chemical composition of dolomite and olivine (wt.%).

Specie	Dolomite	Olivine
Fe_2O_3	2.23	6.9
SiO_2	2.4	41.7
CaO	30.57	0.06
MgO	18.15	49.2
Al_2O_3	0.71	0.45
Na_2O	0.05	-
K_2O	0.158	-
Zn	0.002	-
C	14.64	-
S	0.005	-
NiO	-	0.31
Cr_2O_3	-	0.3

2.3. Kinetic Model Description

A reaction kinetics study provides information on the reaction pathway and whether a reaction is reversible or irreversible as well as the intermediate steps [33]. The kinetics of a thermal reaction can be understood by performing experimental thermodynamic measurements under different operating conditions. Based on the overall reaction order, the rate of reaction depends on the reaction temperature. The rate of reaction (r) is expressed as follows:

$$r \propto [B]^n \tag{2}$$

where $[B]$ is a reactant concentration and n the overall reaction order. The rate of the reaction is proportional to the reaction constant (k):

$$r = k[B]^n \tag{3}$$

$$\frac{d[B]}{dt} = k[B]^n \tag{4}$$

The rate of the reaction in Equation (4) can be given as a function of conversion degree (x):

$$-[B]_o^{1-n} \frac{dx}{dt} = k[1-x]^n \tag{5}$$

A chemical reaction between molecules/particles takes place based on the theory of collision [34]. The E_a of the reaction determines the response of the reaction rate to the temperature and time. The functional form of the mathematical relationship between the reaction constant and absolute temperature ($\overline{T}$) was proposed by Arrhenius in 1889 [33]:

$$k = A \, e^{\frac{-E_a}{RT}} \tag{6}$$

Both pre-exponential constant A and E_a are independent of temperature. By combining Equations (5) and (6), the following equation is obtained:

$$-[B]_o^{1-n} \frac{dx}{dt} = \left[A \, e^{\frac{-E_a}{RT}} \right] [1-x]^n \tag{7}$$

The sample mass loss was used to calculate the conversion degree according to the following formula:

$$x = \frac{m_o - m_t}{m_o - m_f} \tag{8}$$

where m_o, m_t, and m_f are the mass of the sample at the start of the experiment, at the time (t), and at the end, respectively. The TGA was set to work at a constant heating rate (β) which can be introduced to Equation (9) for the non-isothermal conditions:

$$\beta = \frac{dT}{dt} \tag{9}$$

Then, the equation becomes:

$$-[B]_o^{1-n} \frac{dx}{dT} = \frac{A}{\beta} e^{\frac{-E_a}{RT}} [1-x]^n \tag{10}$$

Integration of Equation (10) from an initial to a final value of temperature (T_i and T_f) and conversion (x_i and x_f) allows the E_a in the equation to be estimated as described below:

$$-[B]_o^{1-n} \int_{x_i}^{x_f} \frac{dX}{[1-x]^n} = \frac{A}{\beta} \int_{T_i}^{T_f} e^{\frac{-E_a}{RT}} dT \tag{11}$$

In the present work, the CR method was used to evaluate the Arrhenius parameters [35]. The CR is an integral model-fitting method with good accuracy of estimation. According to Liu et al. [36], the error by the Coats–Redfern method does not exceed $\pm 2\%$ for a conversion degree between 20% and 80%. However, knowledge of the reaction mechanisms (overall reaction order) is required. The following approach was developed by modifying the conventional form to be effective for single or multiple heating rates [37]:

$$\ln\left(\frac{\ln(1-x)}{T^2}\right) = \ln\left[\frac{R\,A}{\beta\,E_a}\left(1 - \frac{2\,R\,\overline{T}}{E_a}\right)\right] - \frac{E_a}{R\,T} \tag{12}$$

where $\overline{T}$ is the arithmetic mean temperature of an experiment. Equation (12) was generalised to be compatible with different reaction mechanisms. It was also assumed that the term $\frac{2\,R\,\overline{T}}{E_a} \ll 1$ to simplify the equation, hence the general form of the method becomes:

$$\ln\left(\frac{G(x)}{T^2}\right) = \ln\left[\frac{R\,A}{\beta\,E_a}\right] - \frac{E_a}{R\,T} \tag{13}$$

The E_a from Equation (13) above can be achieved by plotting term $\ln\left(\frac{G(x)}{T^2}\right)$ against $(1/T)$. The thermal decomposition mechanism function $G(x)$ can be approximated from 19 mechanism models for solid–gas reactions, as listed in Table 3. The accuracy of this method largely depends on the selection of the mechanism function and correlation coefficient (R^2). However, if the E_a is known, the reaction kinetics can be determined. The y-intercept of the E_a in the curve gives the value of the term $\ln\left[\frac{R\,A}{\beta\,E_a}\right]$, which can be rearranged to obtain the A value, as follows:

$$A = \frac{\beta\,E_a}{R} e^{y-intercept} \tag{14}$$

**Table 3.** Typical mechanisms for the solid–gas reaction,(LN: 5235900730034) [38].

Symbol	Reaction Mechanism	$f(x)$	$G(x)$
G1	One-dimensional diffusion, 1D	$1/2x$	x^2
G2	Two-dimensional diffusion (Valensi)	$[-\ln(1-x)]^{-1}$	$x+(1-x)\ln(1-x)$
G3	Three-dimensional diffusion (Jander)	$1.5(1-x)^{2/3}[1-(1-x)^{1/3}]^{-1}$	$[1-(1-x)^{1/3}]^2$
G4	Three-dimensional diffusion (G–B)	$1.5[1-(1-x)^{1/3}]^{-1}$	$1-2x/3-(1-x)^{2/3}$
G5	Three-dimensional diffusion (A–J)	$1.5(1+x)^{2/3}[(1+x)^{1/3}-1]^{-1}$	$[(1+x)^{1/3}-1]^2$
G6	Nucleation and growth ($n=2/3$)	$1.5(1-x)[-\ln(1-x)]^{1/3}$	$[-\ln(1-x)]^{2/3}$
G7	Nucleation and growth ($n=1/2$)	$2(1-x)[-\ln(1-x)]^{1/2}$	$[-\ln(1-x)]^{1/2}$
G8	Nucleation and growth ($n=1/3$)	$3(1-x)[-\ln(1-x)]^{2/3}$	$[-\ln(1-x)]^{1/3}$
G9	Nucleation and growth ($n=1/4$)	$4(1-x)[-\ln(1-x)]^{1/3}$	$[-\ln(1-x)]^{1/4}$
G10	Autocatalytic reaction	$x(1-x)$	$\ln[x/(1-x)]$
G11	Mampel power law ($n=1/2$)	$2x^{1/2}$	$x^{1/2}$
G12	Mampel power law ($n=1/3$)	$3x^{2/3}$	$x^{1/3}$
G13	Mampel power law ($n=1/4$)	$4x^{3/4}$	$x^{1/4}$
G14	Chemical reaction ($n=3$)	$(1-x)^3$	$[(1-x)^{-2}-1]/2$
G15	Chemical reaction ($n=2$)	$(1-x)^2$	$(1-x)^{-1}-1$
G16	Chemical reaction ($n=1$)	$1-x$	$-\ln(1-x)$
G17	Chemical reaction ($n=0$)	1	x
G18	Contraction sphere	$3(1-x)^{2/3}$	$1-(1-x)^{1/3}$
G19	Contraction cylinder	$2(1-x)^{1/2}$	$1-(1-x)^{1/2}$

Note: A–J: Anti–Jander; G–B: Ginstling–Brounshtein.

3. Results

3.1. Effects of Dolomite

The thermal decomposition in CO_2 gasification of Subcoal™ PAF was carried out in the presence of different loadings of dolomite catalysts, as shown in Figure 3a,b.
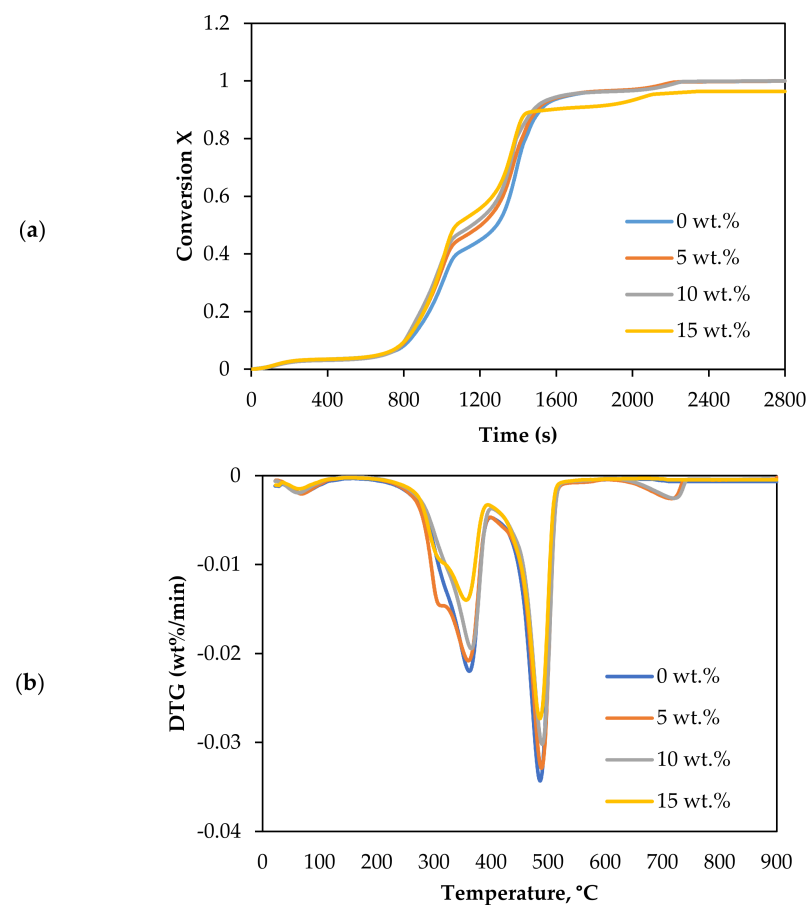
Figure 3. Effect of dolomite loading on the CO_2 gasification: (**a**) conversion degree, and (**b**) DTG curves.

The mass loss of the sample indicates that the rate of decomposition with 15 wt.% dolomite increased more steeply than without the catalyst, as shown in Figure 3a. Additionally, the conversion changed to lower temperature with the addition of the dolomite. The complete conversion reaction decreased from 792.7 to 748.4 °C as the dolomite concentration increased from 0 to 15 wt.%. The sample mainly decomposed in two sub-stages between 200 and 520 °C. Dolomite showed good performance in promoting the reaction rate of CO_2 gasification. It enhances the cracking of tar and increases the production of syngas [39]. However, at the concentration and conditions, dolomite catalysed the CO_2 gasification reaction slightly better than olivine [13].

Table 4 lists the T_m and thermal degradation DTG values. The degradation rate in the first and fourth stages was insignificant compared to the second and third stages (decomposition step). The T_m value reduced with the increase in the dolomite loading. T_m decreased from 484.8 to 477.2 °C as the dolomite loading increased from 0 to 15 wt.%. The DTG at the lowest T_m and 15 wt.% dolomite was -0.0270 wt.%/min.

Table 4. DTG and values of T_m of CO_2 gasification of Subcoal™ PAF with different loadings of the catalyst.

wt.% of Catalyst	Dolomite		Olivine	
	T_m (°C)	DTG (wt.%/min)	T_m (°C)	DTG (wt.%/min)
0	489.3	-0.0322	489.3	-0.0322
5	482.3	-0.0273	488.4	-0.0315
10	479.8	-0.0272	485.5	-0.0292
15	477.2	-0.027	483.8	-0.0285

3.2. Effects of Olivine

CO_2 gasification was conducted in the presence of different loadings of olivine. The decomposition and DTG reaction were plotted as a function of temperature in Figure 4a,b.

The olivine in CO_2 gasification exhibited a similar performance as that in dolomite. The olivine also promoted the decomposition of biomass. It can be seen from Figure 4a; the reaction time decreased as the catalyst loading increased. The complete conversion reaction decreased from 792.7 to 767.7 °C as the olivine concentration increased from 0 to 15 wt.%. The conversion curve also showed two regimes of decomposition: the first was between 0.2 and 0.45, and then from 0.45 to 0.8.

In terms of the DTG analysis, the curves drifted to a lower temperature as the loading of olivine increased. The DTG parameters are listed in Table 4. The value of T_m reduced from 489.3 to 483.8 °C as the catalyst loading increased from 0 to 15 wt.%. Regarding the degradation rate, the peaks decreased from -0.0322 to -0.0285 wt.%/min. The difference between the highest and lowest values of T_m was 5.5 °C at catalyst loadings of 15 wt.% olivine and 0 wt.%.

3.3. Kinetic Analysis

The CR method was used to determine the E_a and A of gasification for different mechanism models ($G(x)$) using Equations (13) and (14). Figure 5 displays the approximated curves of the CR method for ($G(x)$). The linear relationship between Ln ($G(x)/T^2$) and $1/T$ implies a single mechanism reaction. However, most lines showed that the reaction has a multi model mechanism. Furthermore, as the catalyst ratio increased, the reaction lines for all models decreased due to a shorter reaction time, as shown in Figure 5. The comparison of the E_a obtained from each model and test is shown in Figure 6. The effect of dolomite loading on the kinetic parameters was evaluated as listed in Table 5. The table also includes the goodness of fit coefficient to the regression model (R^2) value based on E_a value in order to demonstrate the appropriateness of the model fitting.
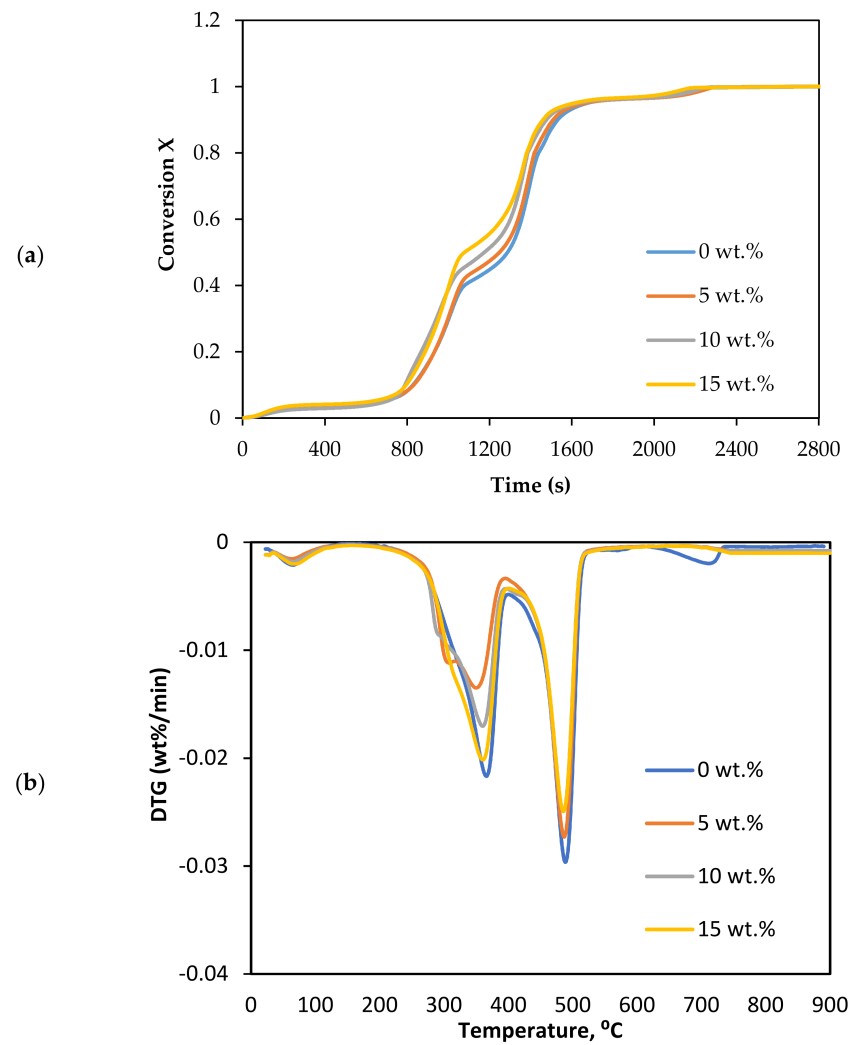
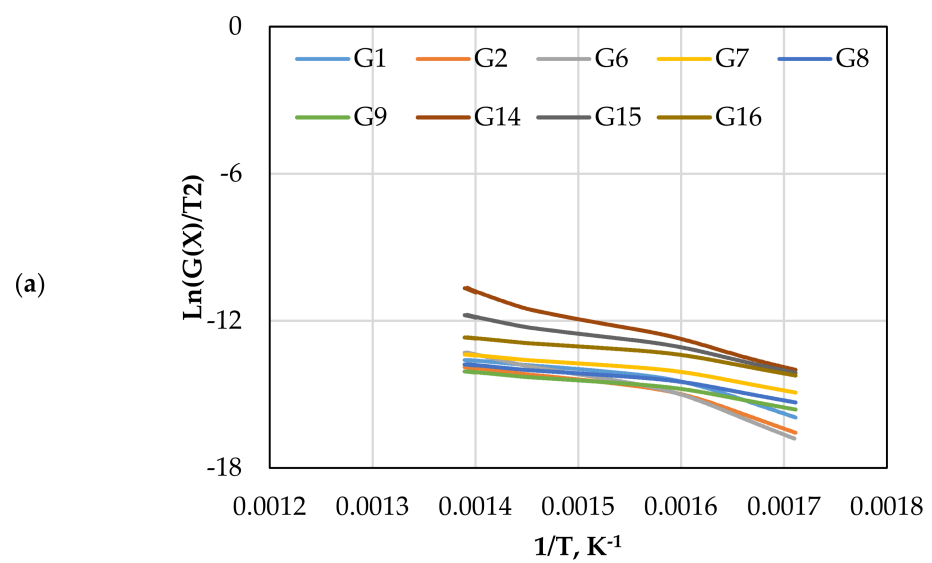**Figure 4.** Effect of olivine loadings on the CO_2 gasification: (**a**) conversion degree, and (**b**) DTG curves.
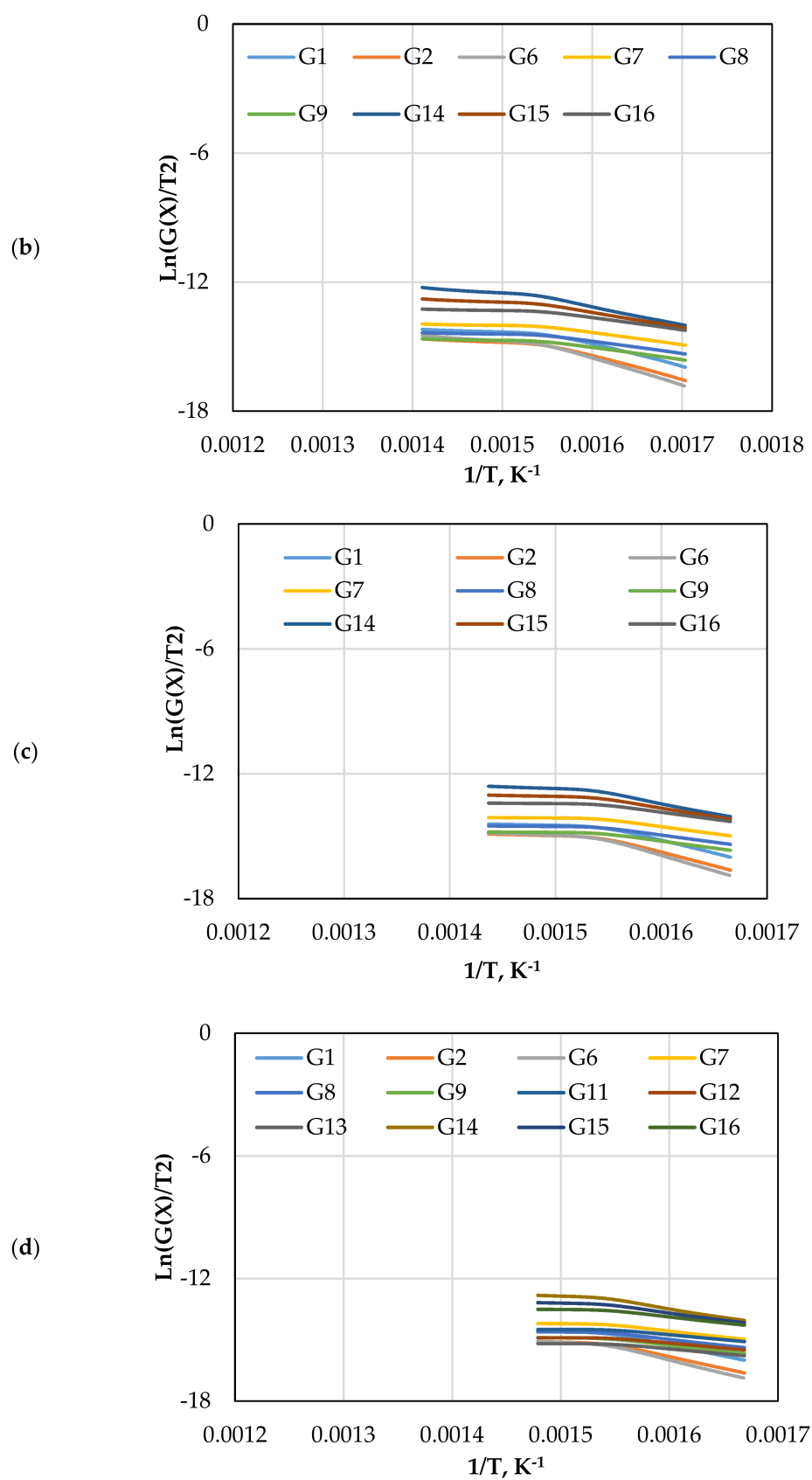

Figure 5. *Cont.*

Figure 5. The CR method plots for CO_2 gasification at different dolomite loadings: (**a**) 0 wt.%, (**b**) 5 wt.%, (**c**) 10 wt.%, and (**d**) 15 wt.%.
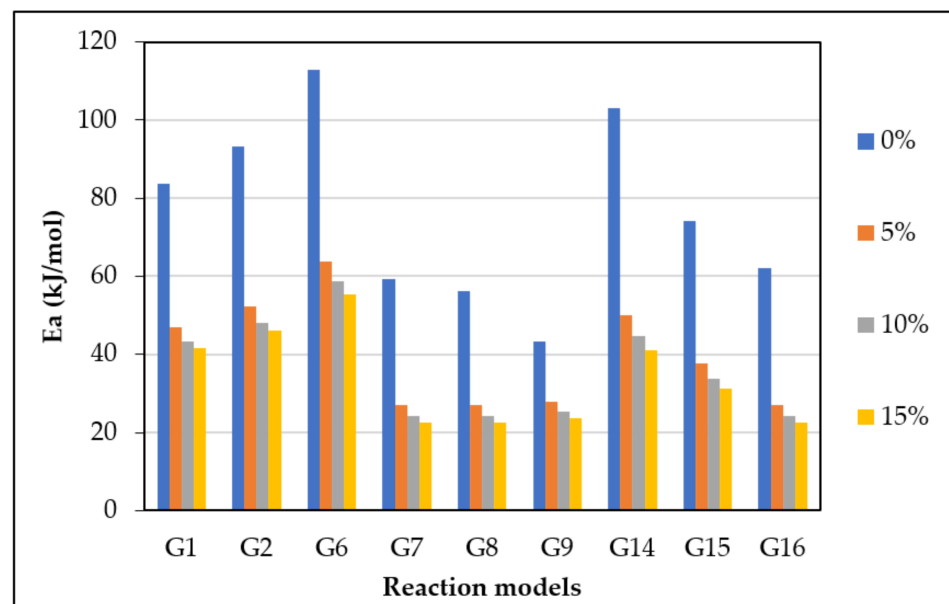
Figure 6. E_a from the most fitting reaction models of CO_2 gasification at different dolomite loadings.

Table 5. Kinetic parameters obtained by CR for the CO_2 gasification of Subcoal™ PAF at different dolomite loadings.

| Model | 0 wt.% | | | 5 wt.% | | | 10 wt.% | | | 15 wt.% | | |
	E_a	A	R^2	E_a	A	R^2	E_a	A	R^2	E_a	A	R^2
G1	83.6	1.3×10^4	0.896	46.9	290	0.883	43.4	110	0.862	41.7	72	0.899
G2	93.3	5.7×10^4	0.918	52.2	520	0.891	48.2	180	0.829	46.1	110	0.858
G6	112.9	6.9×10^6	0.955	63.9	5.5×10^3	0.911	58.6	1.4×10^3	0.852	55.5	660	0.874
G7	59.2	290	0.943	26.9	6.4	0.883	24.2	2.98	0.798	22.6	1.98	0.888
G8	56.2	190	0.943	26.9	4.3	0.882	24.2	2.0	0.798	22.6	1.32	0.898
G9	43.3	140	0.943	27.9	3.2	0.881	25.2	1.5	0.798	23.6	0.99	0.928
G11	-	-	-	-	-	-	-	-	-	15.4	0.28	0.911
G12	-	-	-	-	-	-	-	-	-	13.5	0.16	0.871
G13	-	-	-	-	-	-	-	-	-	13.5	0.12	0.861
G14	103.1	2.9×10^7	0.992	50.1	3.4×10^3	0.941	44.8	890	0.890	41.1	270	0.982
G15	74.2	8.1×10^4	0.980	37.6	180	0.923	33.7	64	0.855	31.2	35	0.949
G16	62.2	570	0.943	26.9	13	0.881	24.2	5.9	0.798	22.6	3.96	0.928

The calculated E_a and A values with the highest R^2 values were 41.1 kJ/mol and 370 min^{-1}, which was found in G14 at 15 wt.% of dolomite loading, as shown in Table 5. However, the other models also showed high R^2 with different values of E_a due to the complexity of the Subcoal™ PAF gasification reactions, and the inhomogeneity of the material. The variation in the E_a was obtained due to the reaction mechanism models, as reported by Aboulkas and El Harfi [40].

Figure 7 displays the reaction kinetic graphs of gasification at different loadings of olivine. Figure 8 and Table 6 compare the values of E_a at various contents of catalyst, which was estimated using different mechanism models. Model G15 at 15 wt.% exhibited excellent linearity with the highest R^2 value of 0.992, which makes it a good candidate for E_a estimation and reaction mechanism.
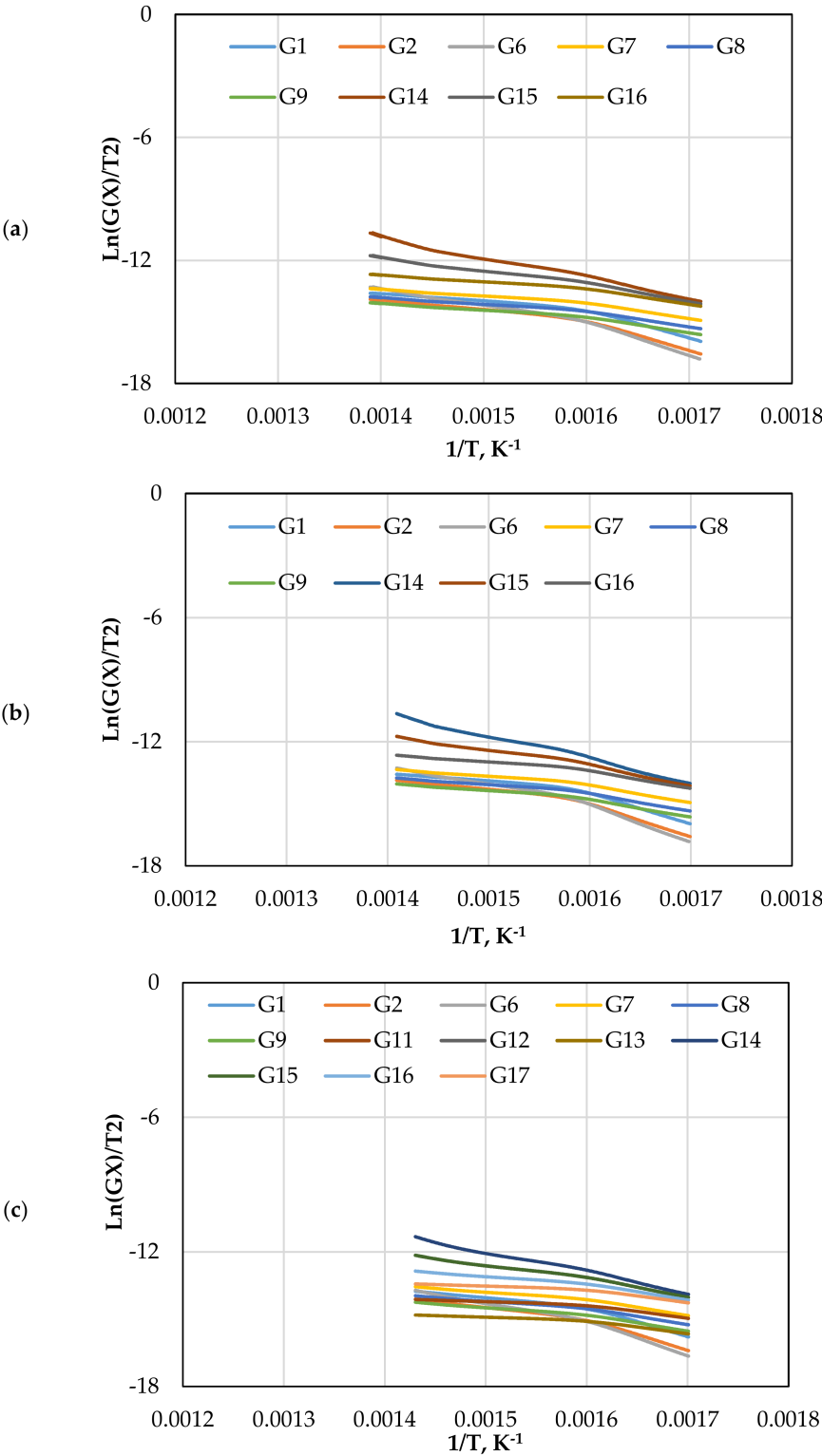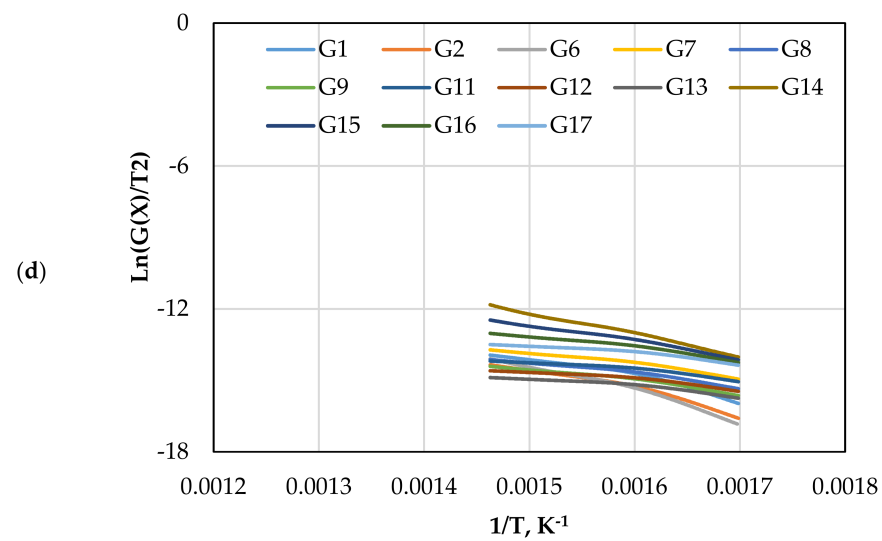
Figure 7. *Cont.*

Figure 7. The CR method plots for CO_2 gasification at different olivine loadings: (**a**) 0 wt.%, (**b**) 5 wt.%, (**c**) 10 wt.%, and (**d**) 15 wt.%.
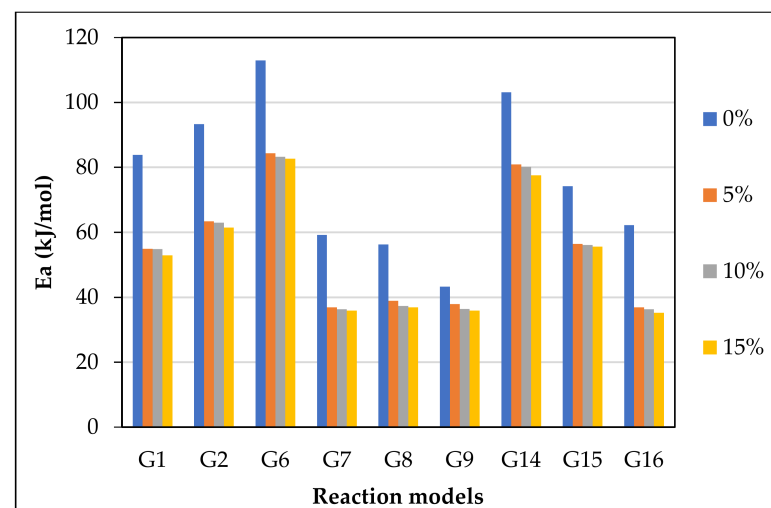

Figure 8. E_a from the most fitting reaction models of CO_2 gasification at different olivine loadings.

Table 6. Kinetic parameters obtained by CR for CO_2 gasification of Subcoal™ PAF at different olivine loadings.

| Model | 0 wt.% | | | 5 wt.% | | | 10 wt.% | | | 15 wt.% | | |
	E_a	A	R^2	E_a	A	R^2	E_a	A	R^2	E_a	A	R^2
G1	83.9	1.3×10^4	0.896	54.9	2.1×10^3	0.904	54.8	2.0×10^3	0.926	52.9	2.7×10^3	0.949
G2	93.3	5.7×10^4	0.918	63.4	7.3×10^3	0.927	62.9	6.4×10^3	0.945	61.4	9.3×10^3	0.965
G6	112.9	6.9×10^6	0.955	84.3	5.4×10^5	0.963	83.2	4.1×10^5	0.975	82.6	6.8×10^5	0.986
G7	59.2	290	0.943	36.9	72	0.950	36.3	62	0.965	35.9	82	0.981
G8	56.2	190	0.943	38.9	48	0.950	37.3	41	0.965	36.9	54	0.981
G9	43.3	140	0.943	37.9	36	0.950	36.4	31	0.965	35.9	41	0.981
G11	-	-	-	-	-	-	23.0	1.8	0.886	22.0	2.2	0.921
G12	-	-	-	-	-	-	23.9	1.2	0.886	21.0	1.5	0.921
G13	-	-	-	-	-	-	21.9	0.91	0.886	21.0	1.1	0.921
G14	103.1	2.9×10^7	0.992	80.9	2.6×10^6	0.993	80.1	1.5×10^6	0.990	77.5	2.7×10^6	0.977
G15	74.2	8.1×10^4	0.980	56.4	1.3×10^4	0.984	56.1	9.4×10^3	0.989	55.6	1.4×10^4	0.992
G16	62.2	570	0.943	36.9	140	0.950	36.3	120	0.965	35.2	160	0.981
G17	-	-	-	-	-	-	23.0	3.7	0.886	22.0	4.4	0.921

4. Discussion

The gasification of Subcoal™ PAF in the TGA occurs according to consecutive steps, namely dehydration, devolatilisation, and char decomposition. In the first step, moisture was removed from a sample at a temperature between 150 to 250 °C. However, in this step, the sample mass insignificantly changed as a function of time. The second step consisted of two stages in which the volatile organic compounds decomposed into condensable and non-condensable gases. This process causes a sudden reduction in a sample mass in a temperature range from 250 to 650 °C [3]. In the final step, a small change in the conversion of biomass was observed due to the decomposition of char into non-condensable gases. The final step occurred from 600 °C to 750 °C. However, as the temperature was below 600 °C, the calcination of dolomite yielded active species such as CaO and MgO, as shown in the reactions (Equations (15) and (16)).
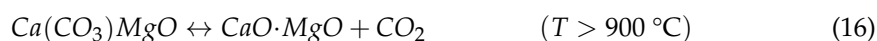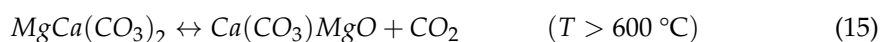
The CO_2 gasification in the presence of dolomite showed lower Tm peaks than olivine. The findings indicate that 15 wt.% of dolomite accelerates the reactions by lowering the Tm of Subcoal™ PAF decomposition. The abnormality of DTG peaks in the second stage can be attributed to the presence of O_2 and interactions of the catalyst [41]. However, the DTG analysis with olivine is quite organised and sharpened compared to the dolomite case [42].

Olivine and dolomite catalysts have a significant and measurable impact on the conversion rate when compared with the heating rate impact [22]. The presence of a catalyst reduced the induction time of the thermal decomposition. It also shifted the conversion curve to a lower temperature as the catalyst concentration increased, indicating a shorter decomposition reaction time. TGA plots of conversion degree were divided into two main degradation regions: 0.2 to 0.45, and then from 0.45 to 0.8. This can be explained by the successive reactions of decomposition.

The accurate estimation of the kinetic parameters of the heterogeneous and non-isothermal reaction is a substantial step in a design of a biomass gasifier. In this work, the model-fitting CR method was used to estimate the E_a and A of the CO_2 gasification process in the presence of olivine and dolomite as catalysts. The method models (G1–G19) were tested to obtain the most fitted graph. In the presence of dolomite or olivine, the E_a was significantly reduced with the increase in the catalyst loading [43]. However, dolomite had a better kinetic performance in comparison with olivine. The degradation process is a chemical reaction-controlled in the first step (reaction extent less than 0.2). In the second and third steps of degradation, when the reaction extent is between 0.2 and 0.8, the process is controlled by three-dimensional diffusion and chemical reaction. Finally, at a reaction extent greater than 0.8, the decomposition is solely controlled by the three-dimensional diffusion mechanism [44]. This reveals that the reaction mechanism of Subcoal™ PAF gasification in the fixed bed is complex and occurs in a multistage thermal decomposition. The higher the complexity of the dehydration mechanism, the greater the variation of E_a [45]. In the DTG analysis, the degradation rate in wt.%/min was plotted against the temperature. Four peaks appeared in the graph showing the amount of degradation that occurred at a specific temperature. Thermal gasification reaction with the catalyst was evaluated according to DTG and Tm values. The results showed two small peaks corresponding to degradation in the first and fourth stages, respectively, as well as two large peaks of the stages in the devolatilisation stage [46]. The Tm peaks overlapped, and the irregularity of the peak shape indicated the occurrence of simultaneous gasification reactions. Additionally, the presence of oxygen in the reaction mixture led to several oxidation reactions that impact the evaluation of DTG. Dolomite has a better degradation performance at constant catalyst concentration than olivine. For model G14, the E_a reduced by 62 kJ/mol as the dolomite concentration increased from 0 to 15 wt.%, while only a 25.6 kJ/mol reduction was obtained by olivine. The lower the E_a, the lower the gasification temperature. For both catalysts, the E_a decreased as the loading of the catalyst increased. The higher the loading of catalysts, the lower the Tm peak obtained [47]. Dolomite causes a higher reduction in Tm value and better DTG outcomes compared with olivine. The fitting of curves showed that models G14 and G15 provided relatively high correlation

coefficient R^2 for both catalysts. The mechanism of the catalytic gasification accordingly varied between second- to third-order chemical reactions. Dolomite enhances tar cracking by promoting the water–gas reaction [48]. The tar elimination in the presence of dolomite can attain 100%, as demonstrated by Simell et al. [17]. Syngas products and an active carbon deposit are formed when a benzene ring is incorporated on the active sites of CaO. The active carbon deposit undergoes a reaction with steam or ends with coke formation on CaO. MgO breaks the H_2 bonding in water, forming OH, which is absorbed on the active sites of MgO. The OH group then combines with the remaining active carbon to form formate. A spill over of OH takes place, leading to decomposition of formate to syngas and the removal of coke [49,50]. Kim et al. [51] carried out a kinetic study on the CO_2 gasification of Chinese low-rank lignite coal and found that the dolomite minimises the E_a and reaction time of biomass gasification.

Dolomite calcination includes the formation of MgO and CaO by thermal cracking [20]. The following chemical reactions describe the calcination of dolomite over two ranges of temperatures [52]:

$$MgCa(CO_3)_2 \leftrightarrow Ca(CO_3)MgO + CO_2 \qquad (T > 600\ °C) \qquad (15)$$

$$Ca(CO_3)MgO \leftrightarrow CaO{\cdot}MgO + CO_2 \qquad (T > 900\ °C) \qquad (16)$$

As can be seen in the reactions, the equilibria of calcination are sensitive to CO_2 gas release. It is preferred that the partial pressure of CO_2 stays under the equilibrium pressure to avoid catalyst deactivation [53]. Besides the process pressure, temperature plays a crucial role in controlling the calcination and carbonation reactions [54]. Other factors that influence the calcination process include heating rate, the quantity of the catalyst, and particle size [55]. The purpose of dolomite calcination is to increase the size of the catalyst pores, which is then responsible for mass transfer enhancement. The time and temperature of calcination increase the surface area of the catalyst, hence the catalysis activity increases [56].

It has been revealed that olivine increases the yield of syngas and tar conversion and reduces the production of CH_4 and CO_2 [12,57]. The gasification in the CO_2 atmosphere causes the oxidation of olivine in the combustion zone, producing binary iron oxide hematite (Fe_2O_3), SiO_2, and iron-depleted olivine. The formed Fe_2O_3 is subsequently reduced by the organic compounds in biomass to FeO, CO, and H_2. In gasification with the synthesis of olivine $(Mg0.5\ Fe0.5)_2\ SiO_4$, about 10% of iron content in olivine is oxidised at 300 s according to thermogravimetric analysis [58]. Moreover, olivine is capable of accommodating excess oxygen from a gasifying agent, as shown in the reaction below:

$$(Mg,\ Fe)_2\ SiO_4 + \frac{\delta}{2}\ O_2\ \rightarrow\ (Mg,\ Fe)_2\ SiO_{4+\delta} \qquad (17)$$
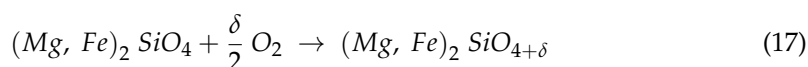
The gained oxygen in olivine is used to partially oxidise methane in the gasification zone when the partial pressure of O_2 is low [58]:

$$(Mg,Fe)_2\ SiO_{4+\delta}\ +\ \delta\ CH_4\ \rightarrow\ (Mg,\ Fe)_2\ SiO_4\ +\ \delta(CO\ +\ 2H_2) \qquad (18)$$
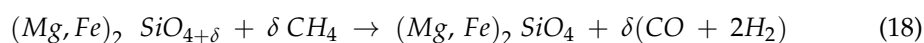
In the CO_2 biomass gasification, olivine undergoes a cycle of oxidation and reduction to produce the active iron and then to regenerate the catalyst. The oxidation of iron in olivine takes place during the calcination at a temperature of 400–1400 °C in two steps. The purpose of olivine oxidation is to produce the Fe_2O_3, wch promotes the tar removal reactions [59].

The crystallinity and mineral content in the Subcoal™ sample and ash may contribute to the catalysis process of CO_2 gasification. The XRF analysis showed that the Subcoal™ ash contained 38 and 18.3 wt.% CaO and Al_2O_3, respectively, which is considered as an effective catalyst of char decomposition reactions [30,60]. The crystallinity of ash and biomass minerals also plays an important role in catalytic activity. Furthermore, there is a

positive correlation between the crystallinity of biomass and decomposition temperature and activation energy [61].

The gasification of MSW, specifically Subcoal™, vitally contributes to the Qatar National Vision 2030 through reducing the MSW landfill and generating renewable power. The availability of naturally occurring minerals in Qatar improves the potential of using Subcoal™ gasification as an alternative to natural gas power plants. Mineral catalysts such as dolomite enhance the gasification efficiency and producer gas quality.

5. Conclusions

- Mineral catalysts can play a vital role in reducing tar formation, operating cost, gasifier size, and improving the producer gas quality and quantity. Herein, the influence of different loadings of olivine and dolomite on the CO_2 gasification of Subcoal™ PAF was examined using TGA.
- The XRD results showed that the crystallinity proportion in Subcoal™ powder and ash was 42% and 37.67%, respectively. The primary crystalline compound in the ash was calcium chloride, which may pose a catalytic effect on the gasification reactions.
- The reaction kinetics and mechanism were evaluated using the CR method at the tested loadings of olivine and dolomite. The findings showed that the decomposition time and temperature decreased as the loading of olivine or dolomite increased from 0 to 15 wt.%.
- For the gasification without a catalyst, G14 was the most appropriate model with the highest R^2 value.
- Dolomite exhibited a better performance in terms of reaction time and mean reaction temperature. Regarding the kinetic evaluation, the probable mechanism model for the gasification reaction at 15 wt.% was G14, which represents the third-order chemical reaction for dolomite. Second-order chemical reaction (G15) showed the highest linearity at 15 wt.% of olivine. The E_a dropped as the loading of the catalyst increased over the ranges tested herein. At 15 wt.% loading, the E_a was 41.1 and 77.5 kJ/mol for dolomite and olivine, respectively.
- Naturally-occurring dolomite is an excellent candidate for promoting large-scale Subcoal™ gasification in Qatar. Gasification of non-recyclable paper and plastic catalysed by dolomite is a sustainable alternative option to mitigate the consequences of global warming and waste landfill in accordance with Qatar National Vision 2030.
- CO_2 as a gasifying agent offers unique features over air or steam to ensure better gasification performance and syngas composition. This work addressed an important aspect of the Subcoal™ gasification catalysis and kinetic parameters. However, further research efforts are required to achieve a full understanding of Subcoal™ gasification.

Author Contributions: Conceptualization, A.M.S.H.A.-M., R.M. and J.S.; Methodology, A.M.S.H.A.-M.; Investigation, A.M.S.H.A.-M.; Resources, A.M.S.H.A.-M.; Writing—original draft preparation, A.M.S.H.A.-M.; Writing—review and editing, R.M. and J.S.; Supervision, R.M. and J.S. All authors have read and agreed to the published version of the manuscript.

Institutional Review Board Statement: Not applicable.

Informed Consent Statement: Not applicable.

Data Availability Statement: Not applicable.

Conflicts of Interest: The authors declare that there are no conflict of interest.

Nomenclature

m_t	Instantaneous mass of sample, (mg)	t	Time, (s)
E_a	Activation energy, (kJ/mol)	$G(x)$	Reaction mechanism model
A	Pre-exponential constant, (min^{-1})	R	Gas constant, (kJ/mol. K)
m_o	Sample mass at the beginning, (mg)	x	Conversion
m_f	Final mass loss of sample, (mg)	k	Rate constant
T	Temperature, (°C)	T_m	Mean temperature, (°C)
R^2	Correlation coefficient	$\overline{T}$	Absolute temperature, (K)

References

1. Mountford, H.; Waskow, D.; Gonzalez, L.; Gajjar, C.; Cogswell, N.; Holt, M.; Fransen, T.; Bergen, M.; Gerholdt, R. COP26: Key Outcomes from the UN Climate Talks in Glasgow. Available online: https://www.wri.org/insights/cop26-key-outcomes-un-climate-talks-glasgow (accessed on 21 December 2021).
2. Magazzino, C.; Mele, M.; Schneider, N. The relationship between municipal solid waste and greenhouse gas emissions: Evidence from Switzerland. *Waste Manag.* **2020**, *113*, 508–520. [CrossRef] [PubMed]
3. Al-Moftah, A.M.S.H.; Marsh, R.; Steer, J. Life Cycle Assessment of Solid Recovered Fuel Gasification in the State of Qatar. *ChemEngineering* **2021**, *5*, 81. [CrossRef]
4. Khan, R. WTE Prospects in the Middle East. Available online: https://www.bioenergyconsult.com/tag/qatar/ (accessed on 21 December 2021).
5. N + P Group. Subcoal® − N + P Recycling. Available online: https://www.np-recycling.nl/en/alternative-fuels/subcoal.html (accessed on 27 September 2021).
6. Syguła, E.; Świechowski, K.; Hejna, M.; Kunaszyk, I.; Białowiec, A. Municipal Solid Waste Thermal Analysis—Pyrolysis Kinetics and Decomposition Reactions. *Energies* **2021**, *14*, 4510. [CrossRef]
7. Bridgwater, A.V.; Beenackers, A.A.C.M.; Sipila, K.; Zhenhong, Y.; Chuangzhi, W.; Li, S. *An Assessment of the Possibilities for Transfer of European Biomass Gasification Technology to China*; Office for Official Publications of the European Communities: Luxembourg, 1999.
8. Islam, M.W. A review of dolomite catalyst for biomass gasification tar removal. *Fuel* **2020**, *267*, 117095. [CrossRef]
9. Tian, Y.; Zhou, X.; Lin, S.; Ji, X.; Bai, J.; Xu, M. Syngas production from air-steam gasification of biomass with natural catalysts. *Sci. Total Environ.* **2018**, *645*, 518–523. [CrossRef]
10. Sirinwaranon, P.; Atong, D.; Sricharoenchaikul, V. Gasification of torrefied cassava rhizome with Ni/MCM-41 catalyst derived from illite waste. *Energy Rep.* **2020**, *6*, 537–547. [CrossRef]
11. DiLoreto, Z.A.; Bontognali, T.R.; Al Disi, Z.A.; Al-Kuwari, H.A.S.; Williford, K.H.; Strohmenger, C.J.; Sadooni, F.; Palermo, C.; Rivers, J.M.; McKenzie, J.A.; et al. Microbial community composition and dolomite formation in the hypersaline microbial mats of the Khor Al-Adaid sab-khas, Qatar. *Extremophiles* **2019**, *23*, 201–218. [CrossRef]
12. Rapagnà, S.; Jand, N.; Kiennemann, A.; Foscolo, P.U. Steam-gasification of biomass in a fluid-ised-bed of olivine particles. *Biomass Bioenergy* **2000**, *19*, 187–197. [CrossRef]
13. Corella, J.; Toledo, J.M.; Padilla, R. Olivine or dolomite as in-bed additive in biomass gasification with air in a fluidized bed: Which is better? *Energy Fuels* **2004**, *18*, 713–720. [CrossRef]
14. Nitsch, X.; Commandre, J.M.; Clavel, P.; Martin, E.; Valette, J.; Volle, G. Conversion of phenol-based tars over olivine and sand in a biomass gasification atmosphere. *Energy Fuels* **2013**, *27*, 5459–5465. [CrossRef]
15. Miccio, F.; Piriou, B.; Ruoppolo, G.; Chirone, R. Biomass gasification in a catalytic fluidized reactor with beds of different materials. *Chem. Eng. J.* **2009**, *154*, 369–374. [CrossRef]
16. Göransson, K.; Söderlind, U.; Engstrand, P.; Zhang, W. An experimental study on catalytic bed materials in a biomass dual fluidised bed gasifier. *Renew. Energy* **2015**, *81*, 251–261. [CrossRef]
17. Simell, P.; Kurkela, E.; Ståhlberg, P.; Hepola, J. Catalytic hot gas cleaning of gasification gas. *Catal. Today* **1996**, *27*, 55–62. [CrossRef]
18. Basu, P. *Biomass Gasification, Pyrolysis and Torrefaction: Practical Design and Theory*; Academic Press: Cambridge, MA, USA, 2018.
19. Dayton, D. Review of the Literature on Catalytic Biomass tar Destruction: Milestone Completion Report. 2002. Available online: https://www.sciencedirect.com/book/9780123964885/biomass-gasification-pyrolysis-and-torrefaction (accessed on 29 September 2021).
20. Richardson, Y.; Blin, J.; Julbe, A. A short overview on purification and conditioning of syngas produced by biomass gasification: Catalytic strategies, process intensification and new concepts. *Prog. Energy Combust. Sci.* **2012**, *38*, 765–781. [CrossRef]
21. Sutton, D.; Kelleher, B.; Ross, J.R.H. Review of literature on catalysts for biomass gasification. *Fuel Process. Technol.* **2001**, *73*, 155–173. [CrossRef]
22. Al-Moftah, A.M.S.H.; Marsh, R.; Steer, J. Thermal Decomposition Kinetic Study of Non-Recyclable Paper and Plastic Waste by Thermogravimetric Analysis. *ChemEngineering* **2021**, *5*, 54. [CrossRef]
23. González-Vázquez, M.D.P.; García, R.; Gil, M.V.; Pevida, C.; Rubiera, F. Unconventional biomass fuels for steam gasification: Kinetic analysis and effect of ash composition on reactivity. *Energy* **2018**, *155*, 426–437. [CrossRef]

24. Rahaman, M.H.A.; Khandaker, M.U.; Khan, Z.R.; Kufian, M.Z.; Noor, I.S.M.; Arof, A.K. Effect of gamma irradiation on poly (vinyledene difluoride)–lithium bis (oxalato) borate electrolyte. *Phys. Chem. Chem. Phys.* **2014**, *16*, 11527–11537. [CrossRef]

25. Marsh, R. *Plastic Film Recycling from Waste Sources*; Cardiff University: Cardiff, UK, 2005.

26. Febrero, L.; Granada, E.; Patiño, D.; Eguía, P.; Regueiro, A. A comparative study of fouling and bottom ash from woody biomass combustion in a fixed-bed small-scale boiler and evaluation of the analytical techniques used. *Sustainability* **2015**, *7*, 5819–5837. [CrossRef]

27. Ward, C.R.; French, D. Determination of glass content and estimation of glass composition in fly ash using quantitative X-ray diffractometry. *Fuel* **2006**, *85*, 2268–2277. [CrossRef]

28. Shoppert, A.; Valeev, D.; Loginova, I.; Chaikin, L. Complete Extraction of Amorphous Alumi-nosilicate from Coal Fly Ash by Alkali Leaching under Atmospheric Pressure. *Metals* **2020**, *10*, 1684. [CrossRef]

29. Kim, S.H.; Lee, C.M.; Kafle, K. Characterization of crystalline cellulose in biomass: Basic principles, applications, and limitations of XRD, NMR, IR, Raman, and SFG. *Korean J. Chem. Eng.* **2013**, *30*, 2127–2141. [CrossRef]

30. Wang, X.; Yao, K.; Huang, X.; Chen, X.; Yu, G.; Liu, H.; Wang, F.; Fan, M. Effect of CaO and biomass ash on catalytic hydrogasification behavior of coal char. *Fuel* **2019**, *249*, 103–111. [CrossRef]

31. Karasmanaki, E.; Ioannou, K.; Katsaounis, K.; Tsantopoulos, G. The attitude of the local com-munity towards investments in lignite before transitioning to the post-lignite era: The case of Western Macedonia, Greece. *Resour. Policy* **2020**, *68*, 101781. [CrossRef]

32. Xiang, Y.; Cai, L.; Guan, Y.; Liu, W.; Cheng, Z.; Liu, Z. Study on the effect of gasification agents on the integrated system of biomass gasification combined cycle and oxy-fuel combustion. *Energy* **2020**, *206*, 118131. [CrossRef]

33. Nakamura, S. Fundamentals of Chemical Reaction Kinetics. In *Solar to Chemical Energy Conversion*; Springer: Berlin/Heidelberg, Germany, 2016; pp. 57–65.

34. Christov, S.G. *Collision Theory and Statistical Theory of Chemical Reactions*; Springer Science and Business Media LLC: Berlin/Heidelberg, Germany, 1980.

35. Coats, A.W.; Redfern, J.P. Kinetic Parameters from Thermogravimetric Data. *Nature* **1964**, *201*, 68–69. [CrossRef]

36. Liu, N.; Chen, H.; Shu, L.; Statheropoulos, M. Error evaluation of integral methods by consideration on the approximation of temperature integral. *J. Therm. Anal. Calorim.* **2005**, *81*, 99–105. [CrossRef]

37. Vyazovkin, S.; Burnham, A.K.; Criado, J.M.; Pérez-Maqueda, L.A.; Popescu, C.; Sbirrazzuoli, N. Kinetics Committee recommendations for performing kinetic computations on thermal analysis data. *Thermochim. Acta* **2011**, *520*, 1–19. [CrossRef]

38. Gai, C.; Dong, Y.; Lv, Z.; Zhang, Z.; Liang, J.; Liu, Y. Pyrolysis behavior and kinetic study of phenol as tar model compound in micro fluidized bed reactor. *Int. J. Hydrog. Energy* **2015**, *40*, 7956–7964. [CrossRef]

39. Cho, M.H.; Mun, T.Y.; Kim, J.S. Air gasification of mixed plastic wastes using calcined dolomite and activated carbon in a two-stage gasifier to reduce tar. *Energy* **2013**, *53*, 299–305. [CrossRef]

40. Aboulkas, A.; El Harfi, K. Study of the Kinetics and Mechanisms of Thermal Decomposition of Moroccan Tarfaya Oil Shale and Its Kerogen. *Oil Shale* **2008**, *25*, 426–443. [CrossRef]

41. Zan, R.; Wang, W.; Xu, R.; Schenk, J.; Zheng, H.; Wang, H. Gasification characteristics and kinetics of unburned pulverized coal in blast furnaces. *Energies* **2019**, *12*, 4324. [CrossRef]

42. Lancee, R.J. Characterization and Reactivity of Olivine and Model Catalysts for Biomass Gasification. 2014. Available online: https://pure.tue.nl/ws/files/3946832/781405.pdf (accessed on 1 October 2021).

43. Marcilla, A.; Beltran, M.; Conesa, J.A. Catalyst addition in polyethylene pyrolysis: Thermogravimetric study. *J. Anal. Appl. Pyrolysis* **2001**, *58*, 117–126. [CrossRef]

44. Vasconcelos, G.D.C.; Mazur, R.L.; Ribeiro, B.; Botelho, E.C.; Costa, M.L. Evaluation of decomposition kinetics of poly (ether-ether-ketone) by thermogravimetric analysis. *Mater. Res.* **2014**, *17*, 227–235. [CrossRef]

45. Wong, F.F.; Lin, C.M.; Chen, K.L.; Shen, Y.H.; Huang, J.J. Improvement of the thermal latency for epoxy-phenolic resins by novel amphiphatic imidazole catalysts. *Macromol. Res.* **2010**, *18*, 324–330. [CrossRef]

46. Nelson, J.B. *Determination of Kinetic Parameters of Six Ablation Polymers by Thermogravimetric Analysis*; National Aeronautics and Space Administration: Washington, DC, USA, 1967.

47. Balasundram, V.; Ibrahim, N.; Samsudin, M.D.H.; Kasmani, R.M.; Hamid, M.K.A.; Isha, R.; Hasbullah, H. Thermogravimetric studies on the catalytic pyrolysis of rice husk. *Chem. Eng. Trans.* **2017**, *56*, 427–432.

48. Yu, Q.-Z.; Brage, C.; Nordgreen, T.; Sjöström, K. Effects of Chinese dolomites on tar cracking in gasification of birch. *Fuel* **2009**, *88*, 1922–1926. [CrossRef]

49. Rigo, V.A.; Metin, C.O.; Nguyen, Q.P.; Miranda, C.R. Hydrocarbon Adsorption on Carbonate Mineral Surfaces: A First-Principles Study with van der Waals Interactions. *J. Phys. Chem. C* **2012**, *116*, 24538–24548. [CrossRef]

50. LaValley, J. Infrared spectrometric studies of the surface basicity of metal oxides and zeolites using adsorbed probe molecules. *Catal. Today* **1996**, *27*, 377–401. [CrossRef]

51. Kim, S.K.; Park, J.Y.; Lee, D.K.; Hwang, S.C.; Lee, S.H.; Rhee, Y.W. Kinetic Study on Low-Rank Coal Char: Characterization and Catalytic CO_2 Gasification. *J. Energy Eng.* **2016**, *142*, 04015032. [CrossRef]

52. Woolcock, P.J.; Brown, R.C. A review of cleaning technologies for biomass-derived syngas. *Biomass Bioenergy* **2013**, *52*, 54–84. [CrossRef]

53. Torres, W.; Pansare, S.S.; Goodwin, J.G., Jr. Hot Gas Removal of Tars, Ammonia, and Hydrogen Sulfide from Biomass Gasification Gas. *Catal. Rev.* **2007**, *49*, 407–456. [CrossRef]

54. Zamboni, I.; Courson, C.; Kiennemann, A. Synthesis of Fe/CaO active sorbent for CO_2 absorption and tars removal in biomass gasification. *Catal. Today* **2011**, *176*, 197–201. [CrossRef]

55. Zhou, C.; Rosén, C.; Engvall, K. Fragmentation of dolomite bed material at elevated tempera-ture in the presence of H_2O & CO_2: Implications for fluidized bed gasification. *Fuel* **2020**, *260*, 116340.

56. Duffy, A.; Walker, G.; Allen, S. Investigations on the adsorption of acidic gases using activated dolomite. *Chem. Eng. J.* **2006**, *117*, 239–244. [CrossRef]

57. Erkiaga, A.; Lopez, G.; Amutio, M.; Bilbao, J.; Olazar, M. Steam gasification of biomass in a conical spouted bed reactor with olivine and γ-alumina as primary catalysts. *Fuel Process. Technol.* **2013**, *116*, 292–299. [CrossRef]

58. Pecho, K.; Sturzenegger, M. Elucidation of the Function of Olivine in Biomass Gasification. 2005. Available online: https://www.osti.gov/etdeweb/servlets/purl/20671631 (accessed on 11 December 2021).

59. Christodoulou, C.; Grimekis, D.; Panopoulos, K.; Pachatouridou, E.; Iliopoulou, E.; Kakaras, E. Comparing calcined and un-treated olivine as bed materials for tar reduction in fluidized bed gasification. *Fuel Process. Technol.* **2014**, *124*, 275–285. [CrossRef]

60. Song, Y.; Hu, J.; Liu, J.; Evrendilek, F.; Buyukada, M. Catalytic effects of CaO, Al_2O_3, Fe_2O_3, and red mud on Pteris vittata combustion: Emission, kinetic and ash conversion patterns. *J. Clean. Prod.* **2020**, *252*, 119646. [CrossRef]

61. Chen, H.; Liu, Z.; Chen, X.; Chen, Y.; Dong, Z.; Wang, X.; Yang, H. Comparative pyrolysis be-haviors of stalk, wood and shell biomass: Correlation of cellulose crystallinity and reaction kinetics. *Bioresour. Technol.* **2020**, *310*, 123498. [CrossRef]